Geochemistry, Geophysics, Geosystems

Supporting Information for

Evolution of the source mineralogy and lithospheric controls on magmatism during the Northeast Atlantic continental breakup

Emily H. Cunningham[1]*, Sarah Lambart[1], Pengyuan Guo[2], Sayantani Chatterjee[3], Christian Tegner[4], Autumn Hartley[1], Ashley M. Morris[1], Sverre Planke[5,6], Christian Berndt[7], Carlos A. Alvarez Zarikian[8], Peter Betlem[6,9,10], Henk Brinkhuis[11,12], Marialena Christopoulou[13], Eric C. Ferré[14], Irina Filina[15], Joost Frieling[16,17], Dustin T. Harper[18], Morgan T. Jones[6,19], Jack Longman[20], John M. Millett[5,6,21], Geoffroy T.F. Mohn[22], Reed P. Scherer[23], Natalia Varela[24], Weimu Xu[25], Stacy L. Yager[26]

[1]MagMaX Laboratory, Department of Geology and Geophysics, University of Utah, Salt Lake City, UT, USA

[2]Institute of Oceanology, Chinese Academy of Sciences, Qingdao, China

[3]Earthquake Research Institute, The University of Tokyo, Bunkyō, Tokyo, Japan

[4]Department of Geoscience, Aarhus University, Aarhus, Denmark

[5]Volcanic Basin Energy Research AS, Høienhald, Oslo, Norway

[6]Department of Geosciences, University of Oslo, Oslo, Norway

[7]GEOMAR Helmholtz Centre for Ocean Research Kiel, Kiel, Germany

[8]International Ocean Discovery Program, Texas A&M University, College Station, TX, USA

[9]Norwegian Geotechnical Institute, Oslo, Norway

[10]Department of Arctic Geology, University Centre in Svalbard, Longyearbyen, Norway

[11] NIOZ Royal Netherlands Institute for Sea Research, Den Burg, Texel, Netherlands

[12]Department of Earth Sciences, Utrecht University, The Netherlands

[13]Department of Earth, Atmosphere and Environment, Northern Illinois University, DeKalb, IL, USA

[14]Department of Geological Sciences, New Mexico State University, Las Cruces, NM, USA

[15]Department of Earth and Atmospheric Sciences, University of Nebraska, Lincoln, NE, USA

[16]Department of Earth Sciences, University of Oxford, Oxford, UK

[17]Department of Geology, Ghent University, Ghent, Krijgslaan 297, 9000, Belgium

[18]Department of Geology and Geophysics, University of Utah, Salt Lake City, UT, USA

[19]Department of Ecology, Environment and Geoscience, Umeå University, Umeå, Sweden

[20]Department of Geography and Environmental Science, Northumbria University, Newcastle Upon Tyne, UK

[21]Department of Geology and Geophysics, University of Aberdeen, King's College, Aberdeen, UK

[22]CY Cergy Paris Université, Sorbonne Université, CNRS-INSU, Institut des Sciences de la Terre de Paris, ISTeP, F-95000 Cergy, France

[23]Department of Earth, Atmosphere and Environment, Northern Illinois University, DeKalb, IL, USA

[24]Department of Environmental Sciences, University of Virginia, Charlottesville, VA, USA

[25]School of Earth Sciences and the Research Ireland Centre for Applied Geosciences, University College Dublin, Dublin, Ireland

[26]Department of Earth and Environmental Sciences, Indiana University, Indianapolis, IN, USA

Contents of this file

Additional Supporting Information (Files uploaded separately)

Supplementary tables. This excel file contains:

- **Table S1.** Major and trace elements compositions of the basalts collected during IODP Expedition 396
- **Table S2**. Partition coefficients used in calculations.
- **Table S3**. Calculated parental magma composition at site U1571/72.
- **Table S4**. alphaMELTS calculations described in Appendix B2.
- **Table S5**. Average and one standard deviation for 5% best fit and all passed mineralogy calculated at each site. All passed values are shown in black; 5% best fit values are shown in blue.
- **Table S6**. Average and one standard deviation of the 5% best-fit and all passed mineralogies calculated at each site for a source composition corresponding to pure DMM. All passed values are shown in black; 5% best fit values are shown in blue.
- **Table S7**. Average and one standard deviation of the 5% best-fit and all passed mineralogies calculated at each site using variable partition coefficients. Source composition for these calculations was DMM + 10% MORB. Variable D calculations consider the uncertainty on the D values presented in Table S2. All passed values are shown in black; 5% best fit values are shown in blue.
- **Table S8**. Average and one standard deviation of the 5% best-fit and all passed mineralogies calculated at each site using only basalts with less than 3 wt.% LOI. Source composition for these calculations was DMM + 10% MORB. All passed values are shown in black; 5% best fit values are shown in blue.

Text S1. Brief petrography of the samples.

Cores recovered at site U1566 consists of 14 basaltic units comprised of one or more individual lava flows with interbedded sedimentary units. The largest of these units is over 50 m thick and consists of 16 individual flows, with flow thickness varying from 0.5 m to over 4 m. The top of the igneous unit is composed of a 1.75m thick heavily altered and brecciated picritic lava flow. While picrite is common in the early products of the NAIP volcanism (~ 61 Ma, Spice et al., 2016), this is the only location on the Vøring plateau where picritic material was recovered. The rest of the unit is predominately composed of aphyric basalt with some minor sections of plagioclase-phyric basalt. A few additional thin interbedded igneous lithologies are also present, all of which are heavily altered, including a layer interpreted as an andesitic pyroclastic unit, and, at the base of the unit, a brecciated basalt that overlies a granitic body thought to represent a shallow intrusion (Gernigon et al., 2024). The groundmass of the basalts, primarily made up of subhedral plagioclase microlites and anhedral clinopyroxenes (Planke et al., 2023b), is also more altered than in basalts collected at other sites. Vesicles are also partially to completely filled in by secondary alteration minerals, including zeolite, clay minerals, and carbonates. The granitic intrusion (56.3 ± 0.2 Ma; Gernigon et al., 2024) and the intra-lava sediments (Planke et al., 2023b) at the base of the lava flow pile have both late Paleocene ages.

Sites U1571 and U1572 are located on the Vøring Marginal High (Figure 1). The western part of the Vøring Marginal High is characterized by an expansive SDR sequence. ODP Hole 642E was drilled into the upper termination of the SDR during Leg 104 (Eldholm et al., 1987) and recovered more than 900 m of basalt. Based on their geochemical and petrological composition, the volcanic succession was divided into an upper 800 m thick tholeiite series and a lower series dominated by basaltic andesite flows (Eldholm et al., 1987). Sites U1571 and U1572 both drilled the upper part of the SDR, but the site locations were chosen to would represent different volcanic emplacement environments (Planke et al., 2017). Based on the morphology of the volcanic surface obtained by seismic reflection, U1571 is interpreted as subaerial volcanism, while the pitted volcanic surface at U1572 is interpreted as being emplaced on a wet substrate leading to phreatomagmatic eruptions (Planke et al., 2023c). While lavas at both sites where initially thought as being potentially emplaced diachronously (Planke et al., 2023c), the geochemistry recovered at both sites suggest they represent the same volcanic sequence. Hence, these two companion sites will be discussed together for the remainder of this work. In comparison to the flows collected at site U1566, basalts are overall less vesicular and less altered. Trace native copper was observed in vesicles and veins (Planke et al., 2023c). Locally, the succession of several chilled margins on a short scale (<1 m) and the presence of pipe vesicles suggest an emplacement similar to the pahoehoe-type lava flows (Walker, 1987). The basalts are predominately aphyric, with some occurrences of plagioclase-phyric sections. The groundmass is made up of subhedral plagioclase microlites and anhedral clinopyroxenes. While the age of the lava flow emplacement has not been precisely determined, several pieces of evidence indicate that they were emplaced soon after the Paleocene-Eocene Thermal Maximum (PETM): (1) the Upper Series has been linked to the uppermost nanoplankton zone NP9 and the NP10

zone (Boulter and Manum, 1989) indicating an age ranging between 55 and 54 Ma (Gradstein et al., 2012); (2) biostratigraphy and carbon isotope ratios indicates that the emplacement of the Lower Series at Hole 642E postdates the PETM (Abdelmalak et al., 2016); (3) the lower series contains dacitic units with similar petrography (Eldholm et al., 1987) than another dacitic flow recovered in post-PETM sediments at Site U1570 and dated at 54.6 ± 1.1 Ma (Morris et al., 2024).

Site U1573 was chosen as presumably representing the late phase of breakup volcanism, with emplacement in a submarine environment (Planke et al., 2023e). Drilling at site U1573 recovered five aphyric basalt sequences separated by sedimentary beds. The top basalt subunit is a highly vesicular lava flow with sparse augite-plagioclase phenocrysts, in a cryptocrystalline groundmass dominated by plagioclase and clinopyroxenes. Downhole subunits consist of aphyric basalts where vesicles have been infilled by the same alteration minerals seen at other sites, with the addition of gypsum and occasionally pyrite. These flows also exhibit subhedral plagioclase microphenocrysts and anhedral clinopyroxene (Planke et al., 2023e).

Basalts recovered from site U1574 have been divided into two distinct subunits, both topped by hyaloclastite, transitioning to aphyric to plagioclase-phyric pillow basalts (Planke et al., 2023d) and suggesting a progressive decrease of the water depth during the emplacement of both subunits. Further downhole, additional plagioclase-phyric pillow basalt transitions to a vesicular aphyric basalt. Downcore, the aphyric basalt shows evidence of magma mingling and late-stage segregation. In both subunits, plagioclase-phyric pillow basalts are characterized by plagioclase microphenocrysts clusters in a cryptocrystalline groundmass (Planke et al., 2023d). Lithostratigraphy and palynology on the igneous units at site U1573 and U1574 both suggest late Early Eocene ages (Planke et al., 2023d,e).

Text S2. Mantle potential temperature calculations

We used PRIMELT3 (Herzberg & Asimow, 2015) to determine the mantle potential temperature on the basalts collected on the Vøring margin (Expedition IODP 396 and ODP 104 Hole 642E). Because PRIMELT3 only corrects for olivine fractionation, it is recommended to be used on basalts with 8 wt.% MgO or more. All basalts at Sites U1571-U572 have MgO content lower than 8 wt.% MgO (Fig. S1). Hence, instead of directly using the basalt compositions for these sites, we used their parental compositions. To estimate the parental compositions, we used alphaMELTS (software: Smith & Asimow, 2005; thermodynamic models: Ghiorso & Sack, 1995; Asimow & Ghiorso, 1998) to calculate fractional crystallization paths that can cover the range of basalt observed these sites (Fig. S15). Calculations were performed with MELTS at fO_2 = FMQ (i.e., the fayalite-magnetite-quartz buffer) and with the corrected spinel thermodynamic model (Ghiorso & Sack, 1991). To be able to cover the full range of composition observed at Sites U1571-U1572, we varied the pressure of crystallization between 1 and 6.5 kbar. Table S3 presents the composition of the calculated parental magmas. For Sites U1571-U1572, we

use these modeled parental magma compositions as PRIMELT3 input values. For all other sites, we used basalts compositions with more than 8 wt.% MgO.

The calculated mantle potential temperatures (T_P) at each sites (Fig. S4) are compared with calculations performed on basalt compositions from Hole 642E (Meyer et al., 2009; Vierek et al., 1988), basalts from East Greenland (the conjugate of the Norwegian margin; Fram & Lesher, 1997), and basalt compositions from samples emplaced on Baffin Island and West Greenland at ~61 Ma (Larsen & Pedersen, 2000, 2009; Spice et al., 2016), which have been interpreted as products of the proto-Iceland mantle plume at this time (Spice et al., 2016). All basalts are assumed to have a constant Fe^{2+}/Fe_t ratio of 0.85 (Tegner et al., 1998) and calculations were done at 7 kbar (i.e., close to the pressure expected at the Moho on the Vøring basin). To test the effect of pressure of fractionation on the estimated T_P, we also performed calculations at 1 bar, but is resulted in a temperature difference <10 °C, that is, much lower than the error on the thermometer ± 40°; Herzberg & Asimow, 2015).

PRIMELT3 aims to constrain the mantle potential temperature (T_P) for anhydrous basalts assuming a peridotitic source (Herzberg & Asimow, 2015). Unfiltered data show highly scattered temperatures with T_P as high as 1675°C. However, most of these outputs had associated warnings pointing toward the presence of pyroxenite (and occasionally volatiles) in the source. Additionally, despite the fact we only used basalt compositions with more than 8 wt.% MgO (or parental magma compositions for Sites U1571-U1572), a number of samples also resulted in a clinopyroxene fractionation warning. Clinopyroxene fractionation, by driving up the FeO content of the magma (Herzberg & Asimow, 2008), will also result in an overestimation of the mantle potential temperature. Among the samples collected during the IODP Expedition 396, only one (U1574A-22R-2, 110–113cm) does not produce any warnings from the software and produces a T_P = 1480°C. Once filtered, samples from Hole 642E result in a reduced range of T_P between 1470°C and 1497°C with an average of 1482°C.

Text S3. Mineralogy of the underplated material and metasomatic veins.

To estimate the mineralogy of metasomatic veins at the base of the lithosphere and of underplated material at the base of the crust, we performed fractional crystallization calculations using alphaMELTS and the primary melt composition obtained with PRIMELT3 (Herzberg & Asimow, 2015) on the MgO-rich sample 396-U1566A-18R-1, 72-74cm. Fractional crystallization paths were calculated with MELTS at a pressure of 7 kbar (i.e., Moho depth) and 19 kbar (i.e., base of the lithosphere). We performed calculations at f_{O2} = FQM (i.e., the fayalite-magnetite-quartz buffer). We used the corrected versions of the garnet (Berman & Koziol, 1991) and spinel (Ghiorso & Sack, 1991) models. Calculations failed for F < 7% for calculations run at 19 kbar. However, because the calculated mode for the accumulated cumulates differed by less than 1% between F = 7% and F = 2% at 7 kbar, we can assume that the results would be very similar if full crystallization was reached. Table S4 presents the composition of basalt and primary melt, as well as the accumulated mineral proportions in the fractionated cumulates at each pressure.

Text S4. Constraints on magmatic flux

The magma volume flux (Q_m) of the Icelandic plume during the continental break-up (~54 Ma) was estimated to 55 m^3/s before rapidly decreasing to 4 m^3/s at 40Ma (Mjelde & Faleide, 2009). Assuming the densities of solid and melt are comparable within the uncertainties of the calculation, the magma volume flux can be converted to plume volume flux (Q_v) by dividing Q_m by the total melt fraction at the top of the melting region. The plume volume flux is then be related to the radius of the plume by:

(eq. S1) $$Q_v = \frac{\pi g R^4 \Delta\rho}{8\mu},$$

where g is the gravitational acceleration, R is the conduit radius, and μ is the viscosity of the plume (=10^{20} Pa.s; Brown & Lesher, 2014), and Δρ is the density difference between the mantle plume and ambient mantle created by the thermal anomaly such as:

(eq. S2) $$\Delta\rho = \rho\alpha\Delta T_P$$

With ρ representing density of the mantle. $\Delta T_P = T_P - T_{P0}$ where T_P is potential temperature, T_{P0} is the potential temperature of ambient mantle, and α is the coefficient of thermal expansion (= $3*10^{-5}$; Phipps Morgan, 2001).

The ambient mantle potential temperature (T_{P0}) is best defined as the T_P which is required to produce mid-ocean-ridge basalts (MORB) at spreading ridges. Estimates of ambient T_{P0} vary from 1280 °C (McKenzie & Bickle, 1988) to 1500 °C (Presnall & Gudfinnsson, 2011). This variability reflects the underlying difficulties in assessing T_P. Here we use an estimate of ambient T_{P0} of 1350 °C, which is the value most recently given by Herzberg and Asimow (2015).

We used Melt-PX (Lambart et al., 2016) to model the adiabatic decompression of a pure lherzolitic mantle and to calculate the melt fraction at the top of the melting column. Considering a mantle lithospheric thickness of 60 km (Fernández et al., 2004) and assuming melting stopped at the base of the lithosphere, we performed calculations for various plume radii (Fig. S16). Using equation S1, the peak of magmatic productivity would require a plume conduit radius systematically larger than 100km for $T_P \leq 1500$°C (i.e., $\Delta T_P \leq 150$°C). Decreasing the T_P, adding dense recycled material in the plume, or considering a temperature gradient in the plume, will all require an even larger plume conduit to produce the same magmatic flux. Geodynamic predictions typically suggest that well-developed plumes should have conduits of no more than 100 km in radius (e.g., Richards et al., 1989; Steinberger & Antretter, 2006). In addition, while the radius of the plume conduit beneath Iceland today is not very well constrained (e.g., Allen et al., 1999 and references therein), recent models favor plume conduit radius smaller than 100km (e.g., Ribe et al., 2020; Steinberger & Antretter, 2006).

Finally, we also acknowledge that those simple calculations are for anhydrous source. However, while the presence of volatiles in a mantle source can result in significantly depressing its solidus (e.g., Asimow & Langmuir, 2003; Dasgupta & Hirschmann, 2006), it

does not significantly affect the total magmatic productivity (Katz et al. 2003). In the context of a mantle plume, the presence of volatile in the source could slightly increase the buoyancy of the plume by decreasing $\Delta\rho$, and consequently its magmatic productivity, but would also result in lower calculated potential mantle temperature (Lee et al., 2009). Hence, we believe that adding volatiles in the source will not be able to simultaneously conciliate constraints on both Q_m and T_P.

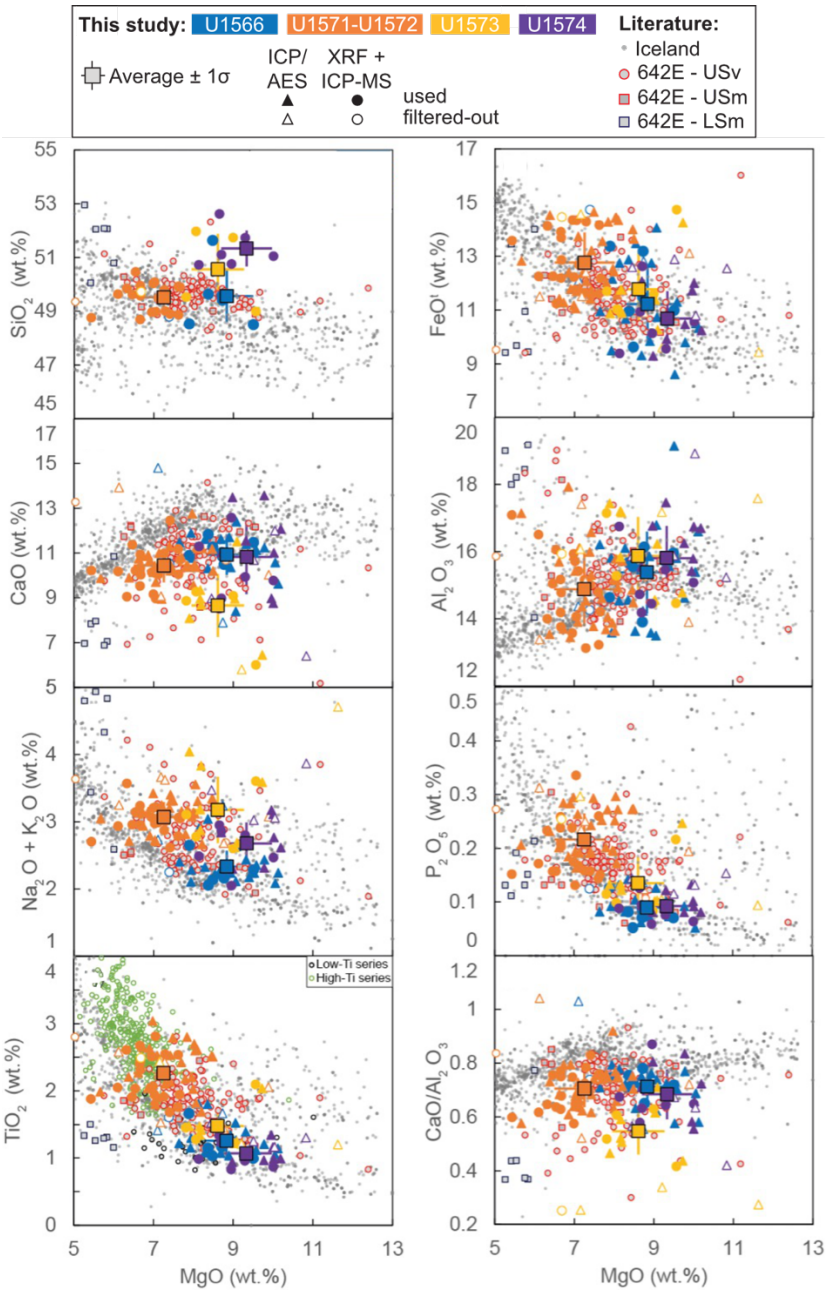

Figure S1. Major element compositions of the basaltic samples collected during IODP Exp. 396. Data sourced from Tegner et al. (2025). Only samples with more than 5 wt.% MgO and less than 5 wt.% LOI are plotted. U1566 samples are in blue, U1571 and U1572 in orange, U1573 in yellow, and U1574 in purple. Circles are XRF analyses, triangles are ICP-AES

analyses. The large squares with error bars represent the average concentration at each site and the associated one standard deviation. Filled symbols were used to calculate the average, open symbols were filtered out (see section 3.2 for more details). For comparison, basalt compositions from IODP Hole 642E (USv = upper series from Viereck et al., 1989; USm and LSm = upper and lower series from Meyer et al. (2009) for samples with < 53 wt.% SiO2) and Iceland (Harðardóttir et al., 2022) are also plotted. In (g), the east Greenland flood basalt low-Ti and high-Ti series from Tegner et al. (1998) are also plotted. All compositions are renormalized to 100 wt.% anhydrous.

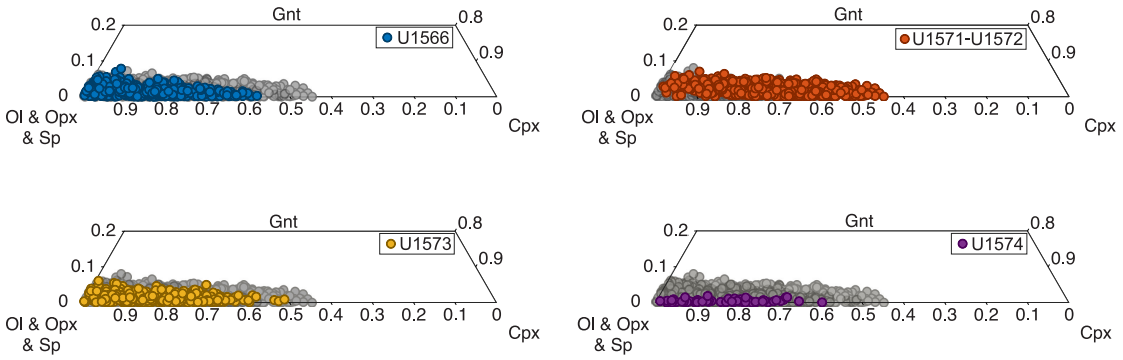

Figure S2. Additional ternary projection. Outputs from calculations presented in Figure 5 showing garnet and clinopyroxene variations independently.

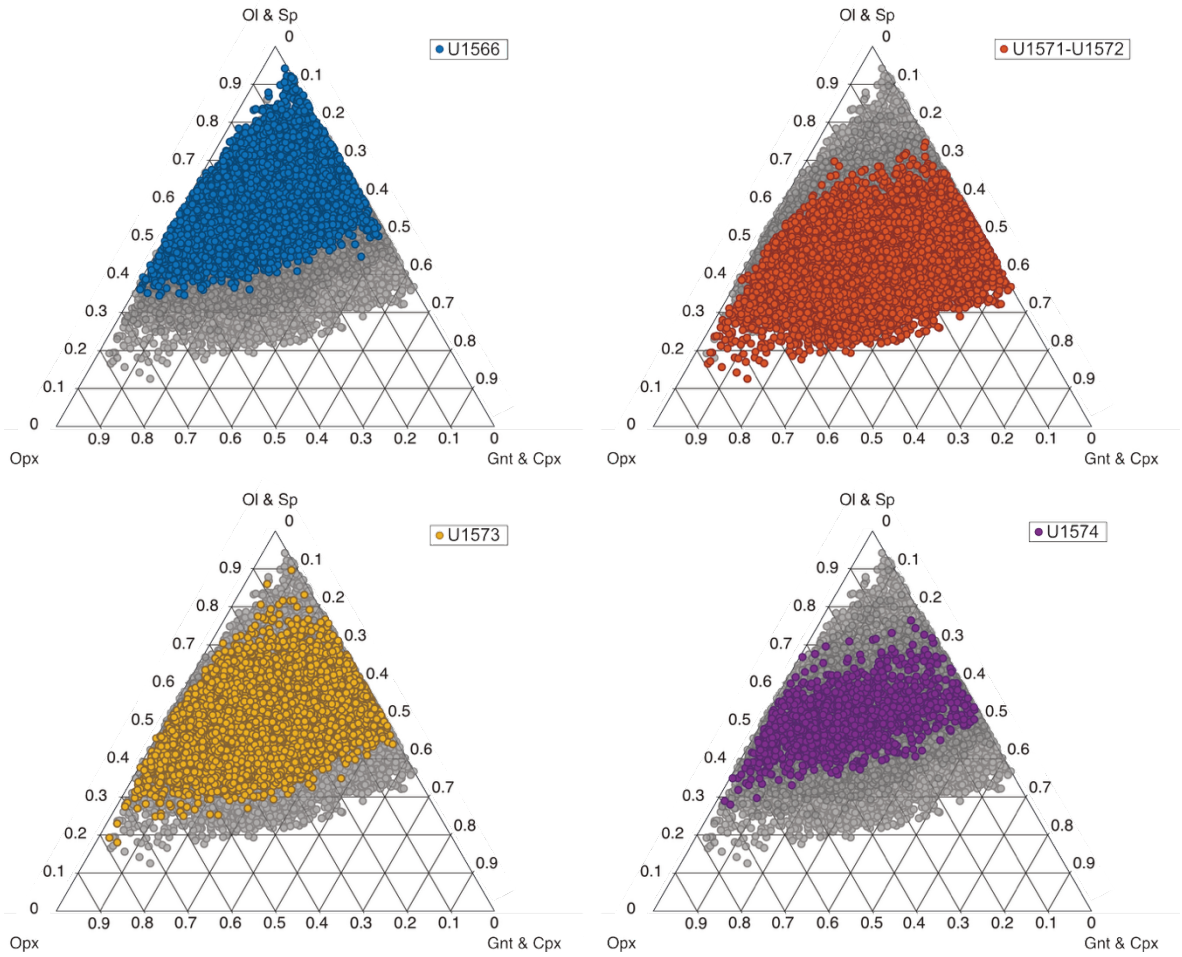

Figure S3. All passed mineralogies. All modeled mineralogy outputs represented in Figure 5. Grey circles show the passed mineralogies for the three other sites on each plot.

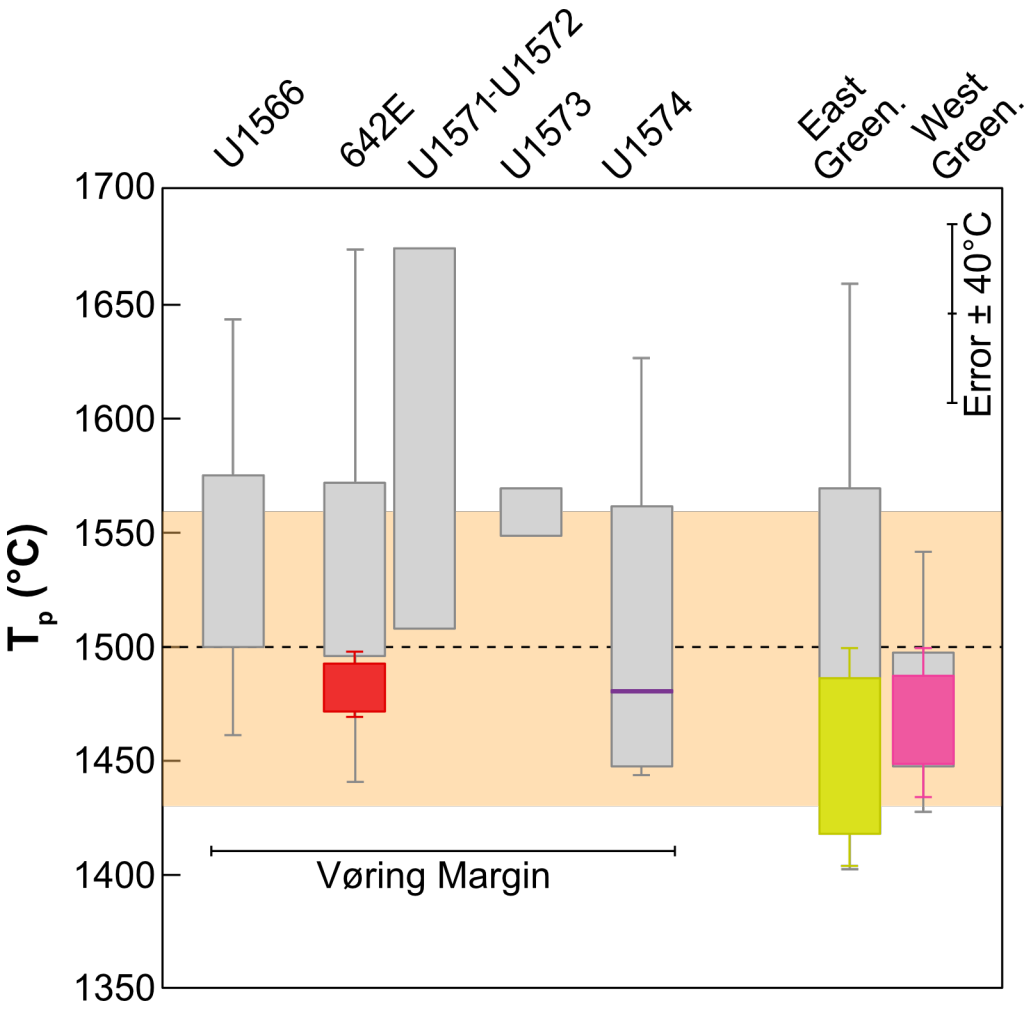

Figure S4. **Calculated mantle potential temperatures (T_P).** T_P calculated with PRIMELT3 (Herzberg & Asimow, 2015) for the Vøring Margin (including data from ODP Hole 642E; Meyer et al., 2009; Viereck et al. 1988), compared to calculated temperatures for West (Larsen & Pedersen, 2009; Spice et al., 2016) and East (Fram & Lesher, 1997) Greenland. All calculations are performed on basalt with more than 8 wt.% MgO with $Fe^{2+}/Fe_t = 0.85$ and at a pressure of 7 kbar. Grey boxes are estimations before filtering. Colored boxes are temperatures obtained only on aphyric lavas that did not produce any warnings. The dashed line marks the maximal T_P after filtering. Orange shaded area is the temperature range estimated by Brown and Lesher (2014) required to explain both the crustal thickness and the isotopic compositions of the East Greenland lavas in the presence of a mantle plume.

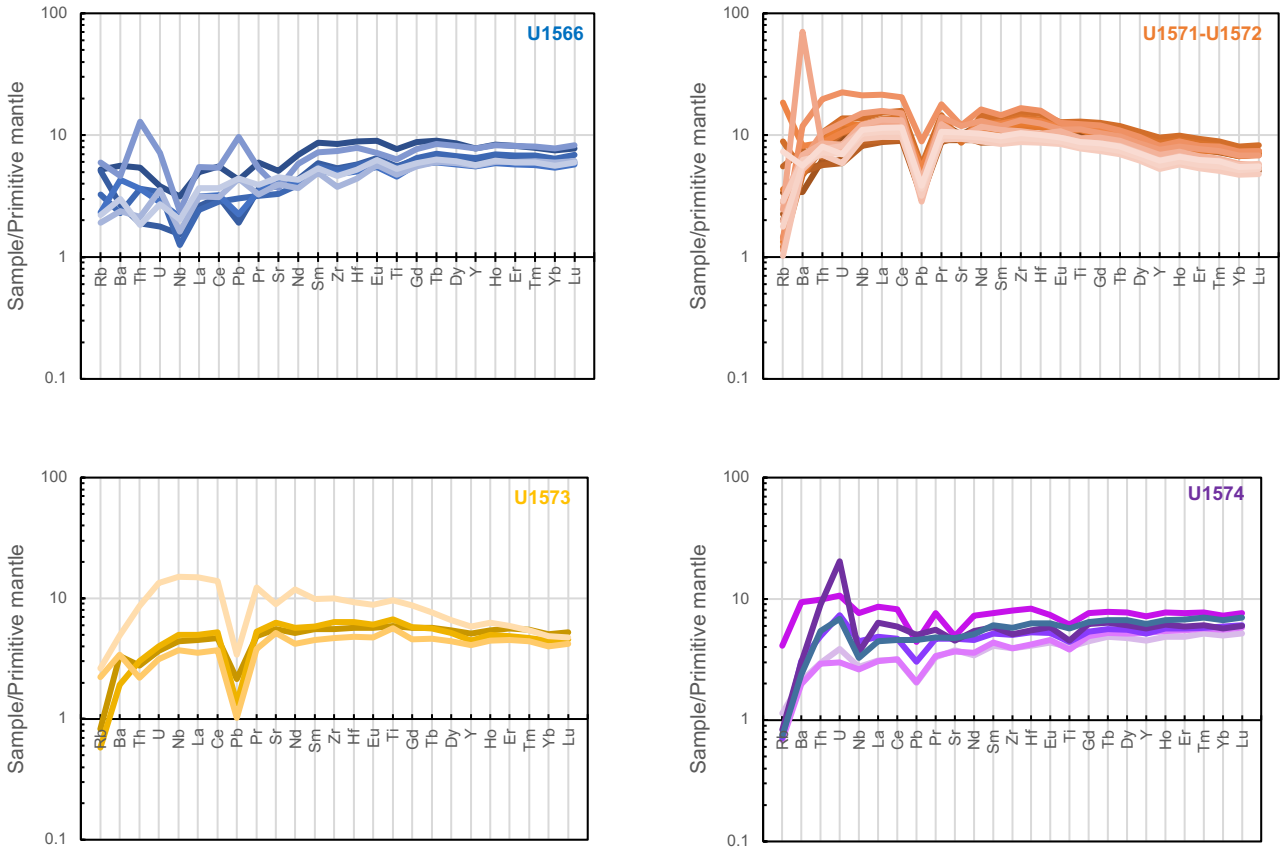

Figure S5. Primitive mantle normalized incompatible trace element variation diagram for each site. The normalizing values of Sun and McDonough (1989) were used.

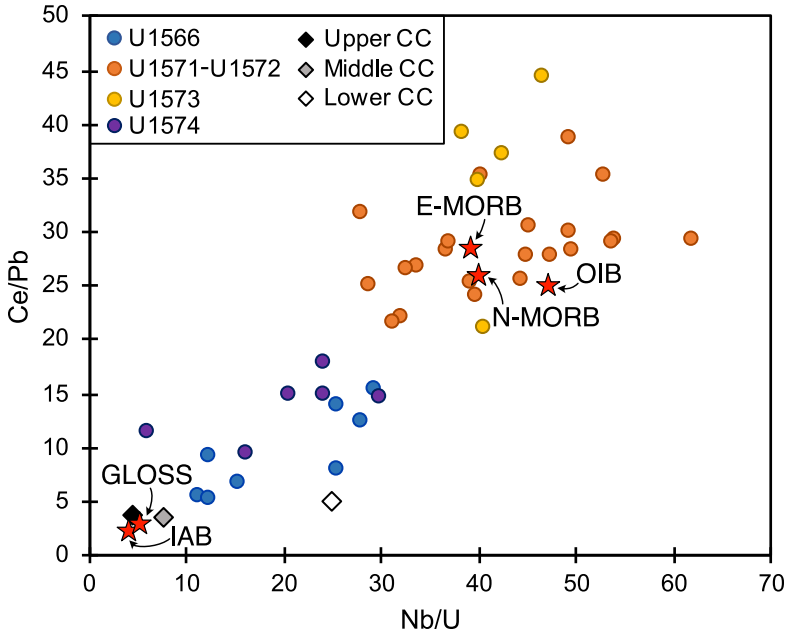

Figure S6. Crustal contamination plot. Ce/Pb vs Nb/U scatter plot showing IODP Exp. 396 samples compared to continental crust, common basalt suites, and GLOSS. Low ratios for samples collected from Sites U1566 and U1574 show that samples likely suffered some crustal contamination. Continental crust data from Rudnik and Gao (2003); OIB data from Sun and McDonough (1989); N- and E-MORB from Niu et al. (2002); IAB data from Niu and O'Hara (2003); GLOSS from Plank and Langmuir (1998). Figure modeled after Quanshu and Xuefa (2014).

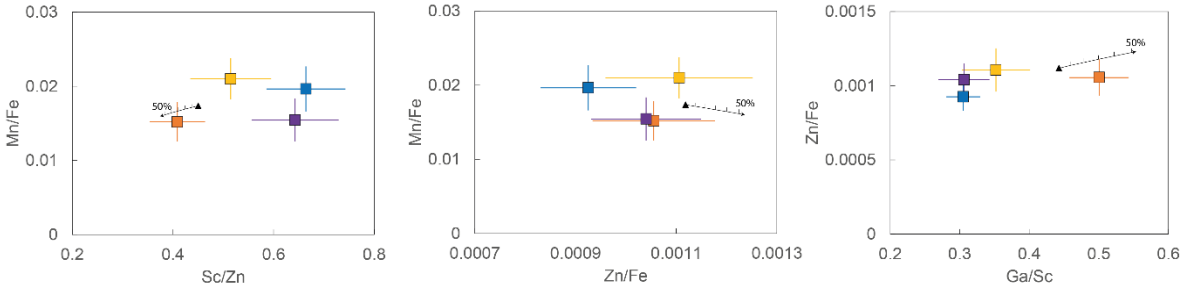

Figure S7. Magma mixing plot. Mixing trends between a N-MORB (black triangle; Gale et al., 2013) and up to 50% continental crust (Rudnick & Gao, 2003) compared to the average basalt compositions at each site and their associated one standard deviation for the elemental ratios used in the Monte Carlo approach.

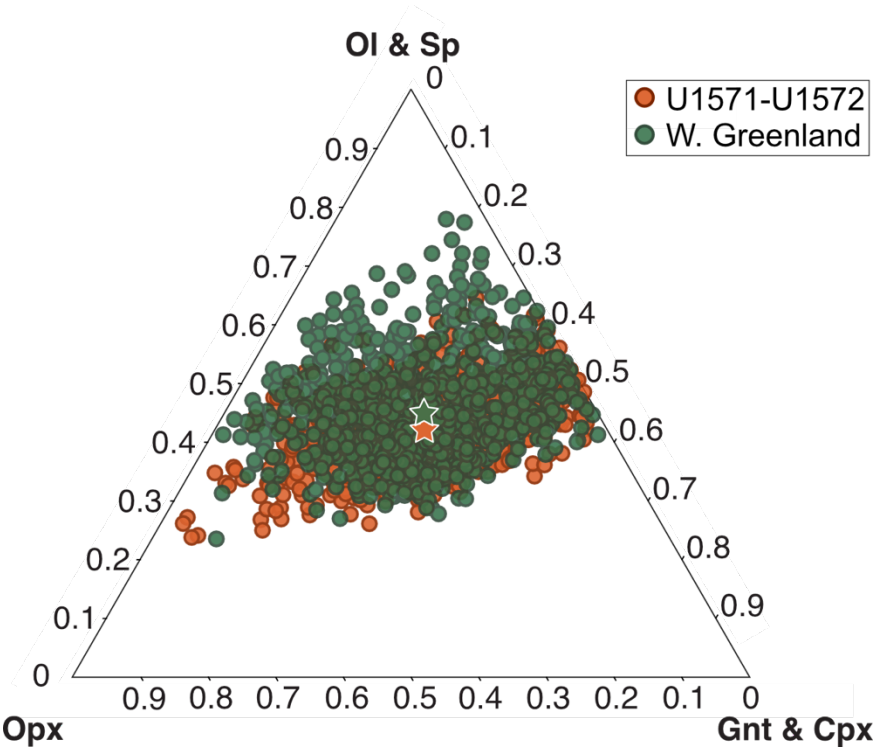

Figure S8. Comparison of the best-fit mineralogies between Site U1571-U1572 and West Greenland. Comparison plot made using the same number of outputs from each site. Star symbols represent the average calculated mineralogy for each Site. The density plot for all passed mineralogy for West Greenland is presented in Figure 8 in the manuscript.

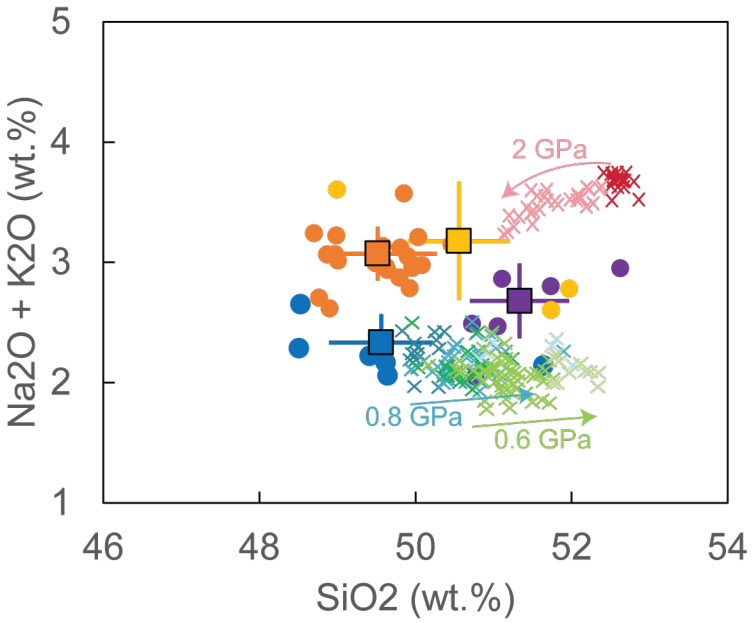

Figure S9. Measured basalt compositions compared to theoretical melt compositions. Basalt compositions collected during IODP Exp. 396 (same symbols and colors as in Figure S1) compared with melt compositions resulting from interaction between a tholeiitic magma and a peridotite (crosses) at various pressures. Experiments at 0.8 and 0.6 GPa (GB40 and GB44, respectively) are from van den Bleeken et al. (2011) and show the evolution of the melt through percolation of a peridotite layer (dark symbols are initial melt composition, intermediate symbols are melt analyses perform in the peridotite layer, and light symbols are melt analyses performed in a melt trap after the peridotite layer). The 2 GPa experiment shows the reaction between a tholeiitic melt and harzburgite (see Fig. 5 in Hou et al., 2024). Dark symbols show the initial melt composition, light symbols show the evolution of the melt toward the peridotite layer for a 2-hour experiment.

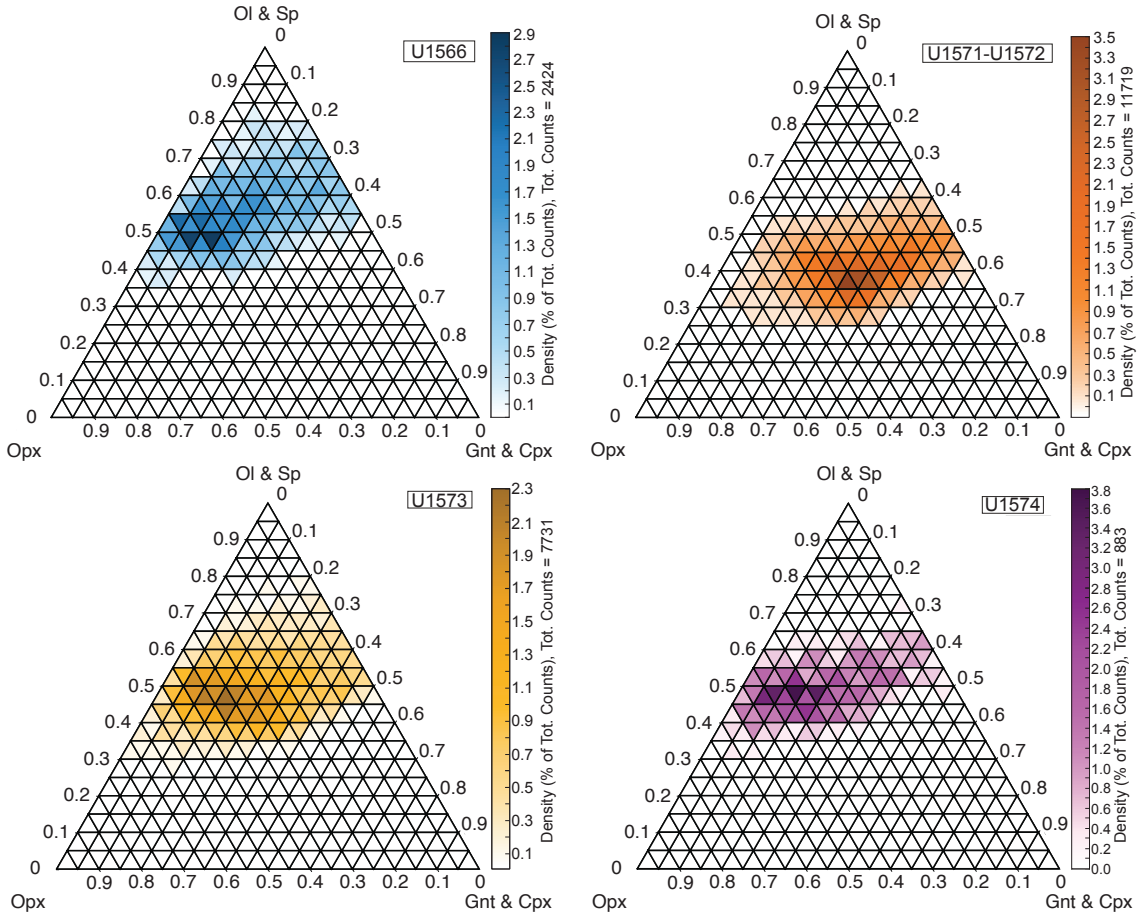

Figure S10. Ternary density plot for basalts with less than 3 wt.% LOI. Averages and standard deviations of outputs are presented in Table S8.

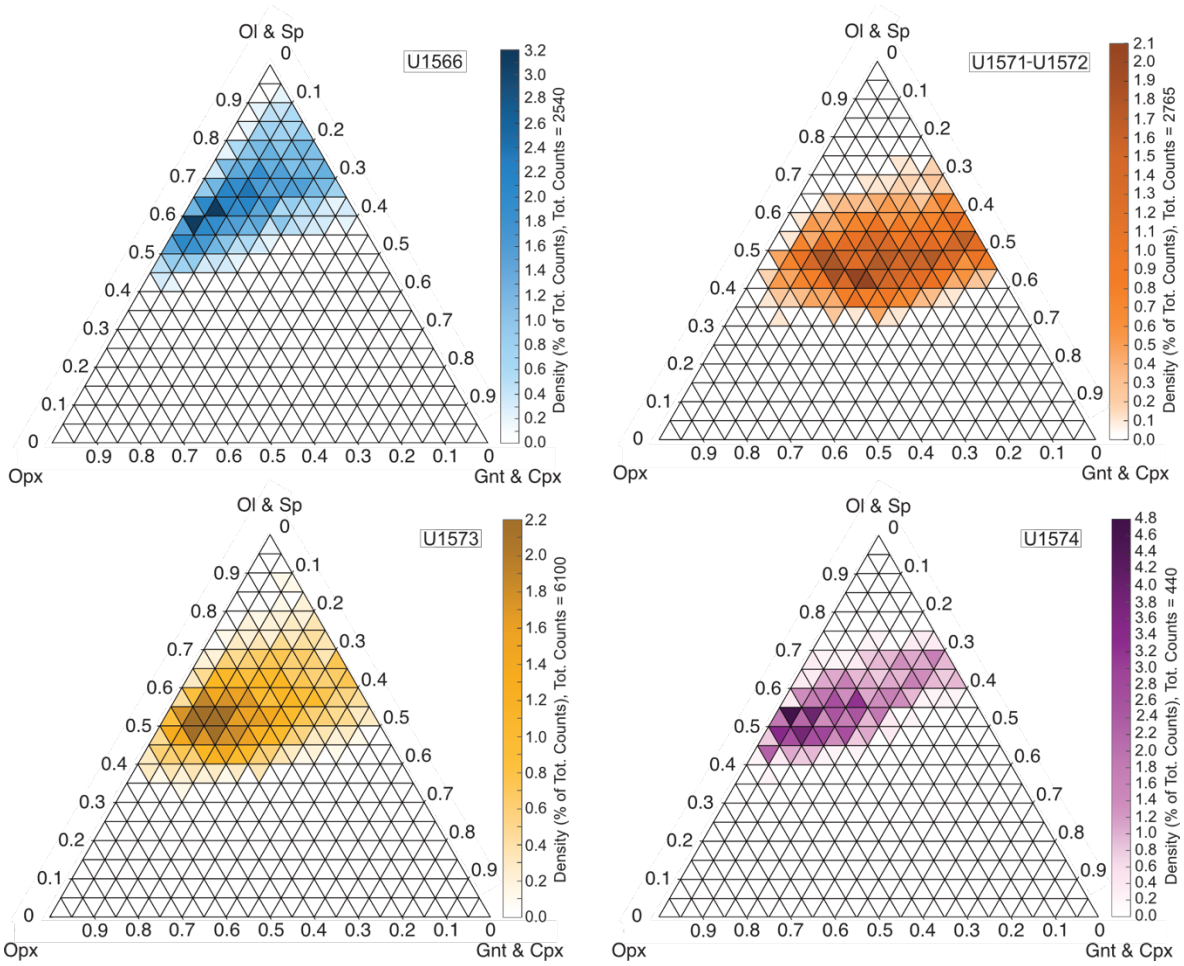

Figure S11. Density plot obtained using Cr_0 corresponding to pure DMM. The other parameters are the same as in Figure 5. Total numbers of passed mineralogies are 2540 for sites U1566, 2765 for sites U1571-U1572, 6100 for site U1573, and 440 for site U1574. Color scale indicates density as a percent of total number of outputs. DMM values from Salters and Stracke (2004).

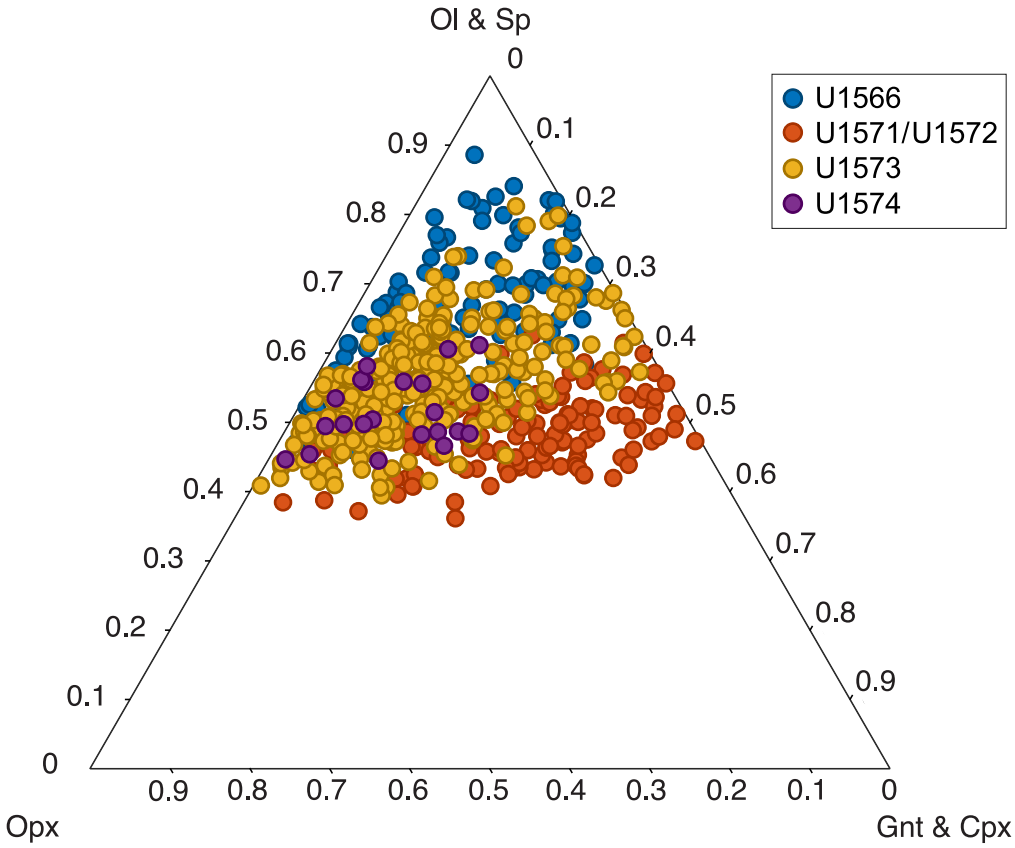

Figure S12. 5% best-fit mineralogies using Cr0 corresponding to pure DMM. The other parameters are the same as in Figure 5. DMM values from Salters and Stracke (2004).

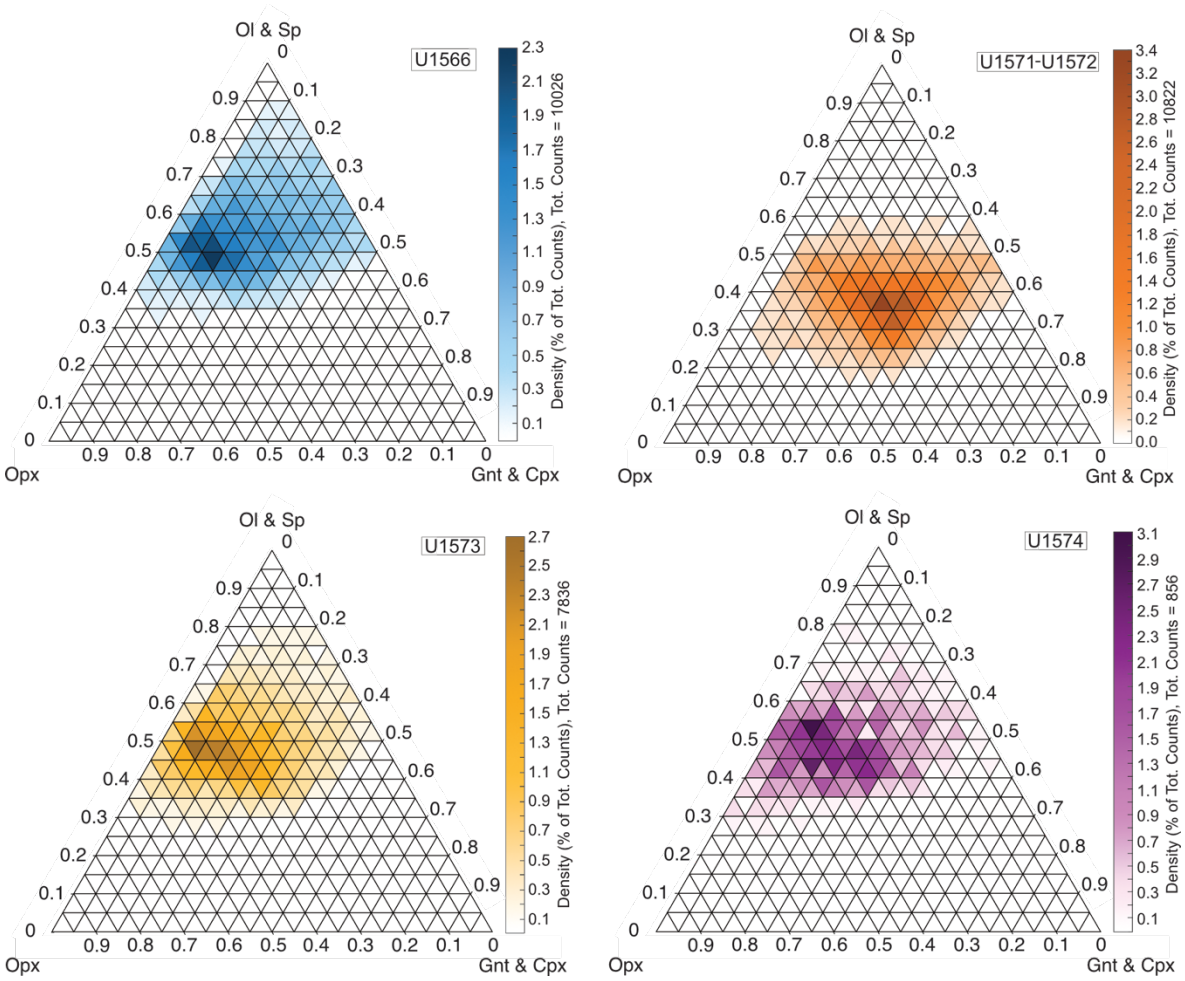

Figure S13. Variable partition coefficient outputs – density plot. Ternary density plot obtained when uncertainty on Ds (Table S2) is taken into account in the model. The other parameters are the same as in Figure 5. Total numbers of passed mineralogies are 10026 for sites U1566, 10822 for sites U1571-U1572, 7836 for site U1573, and 856 for site U1574. Color scale indicates density as a percent of total number of outputs.

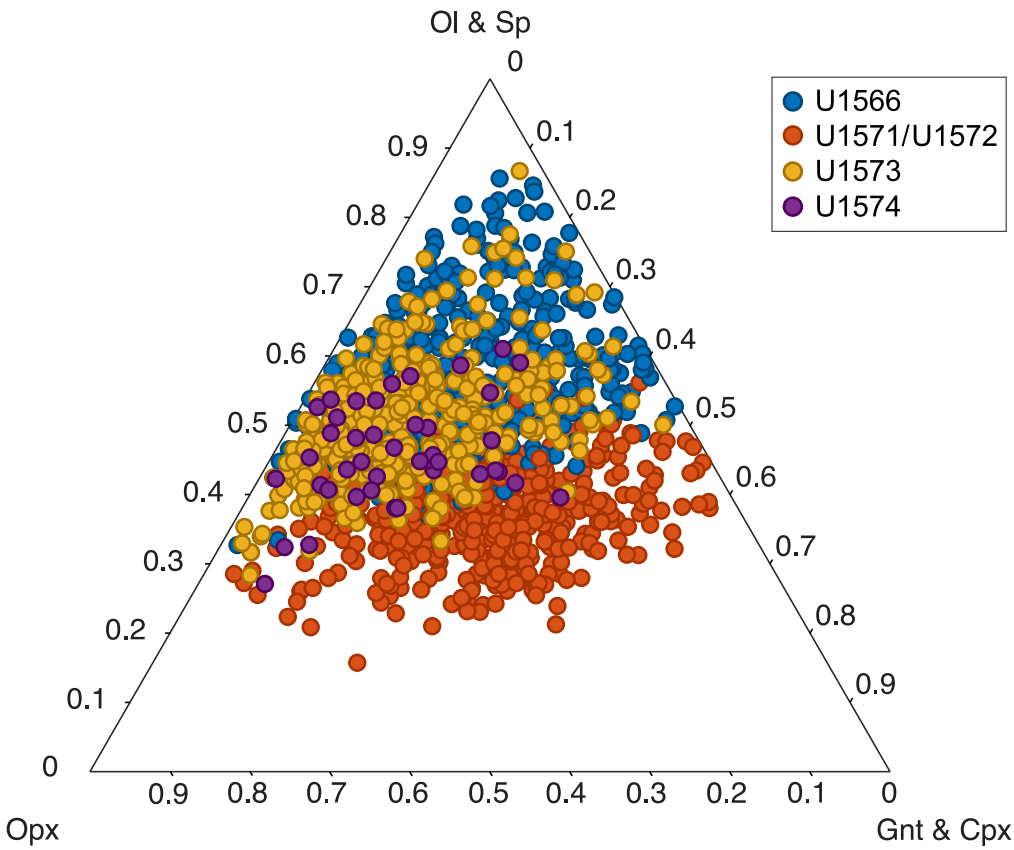

Figure S14. Variable partition coefficient outputs – scatter plot. 5% best-fit mineralogies obtained when uncertainty on Ds (Table S2) is taken into account in the model. The other parameters are the same as in Figure 5.

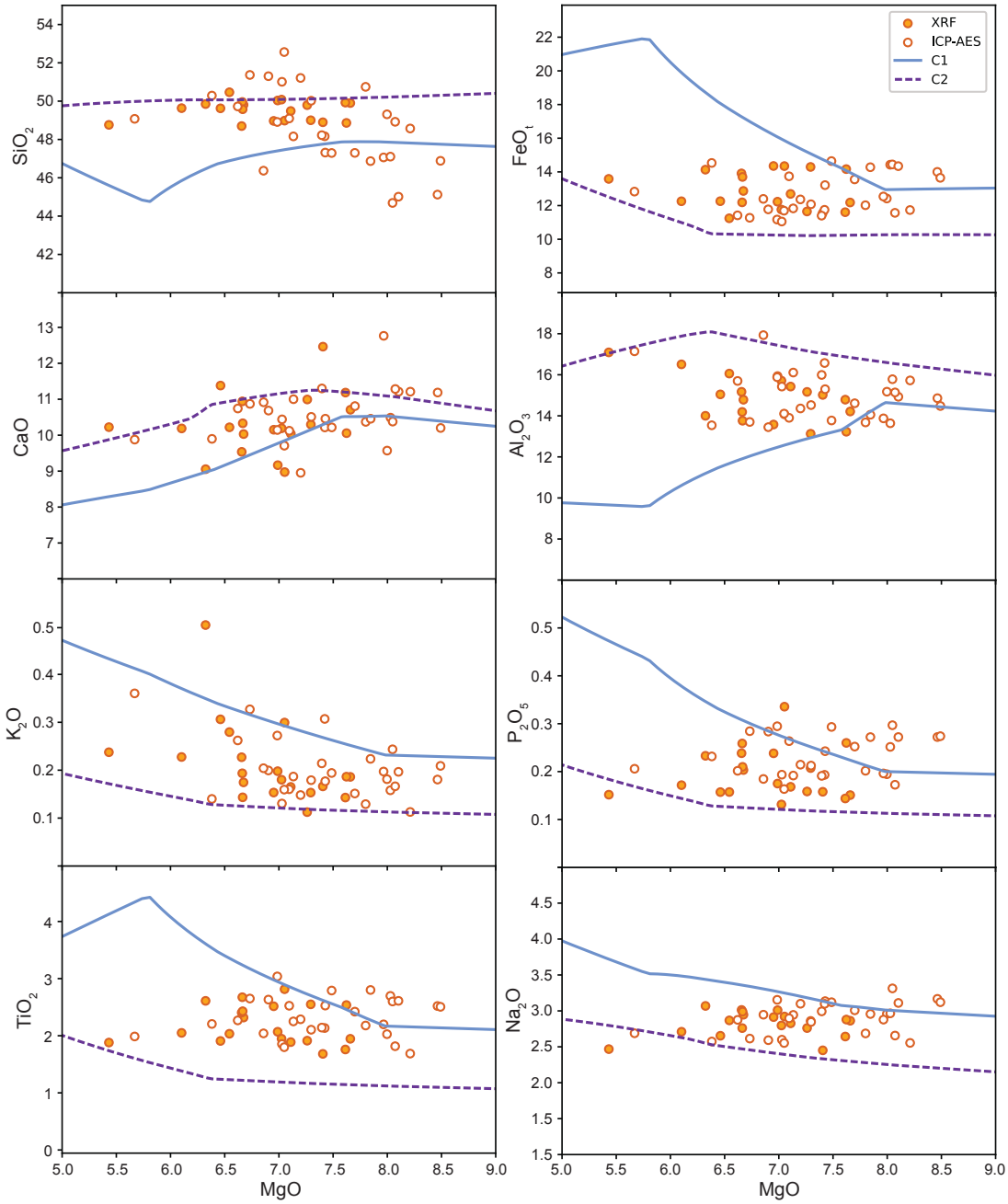

Figure S15. Harker plots depicting the fit of calculated parental magma compositions for Sure U1571-U1572. Parental magma compositions calculated using alphaMELTS (see Appendix B). Compositions C1 and C2 (Table S3) are the compositions used as input for this site in PRIMELTS calculations.

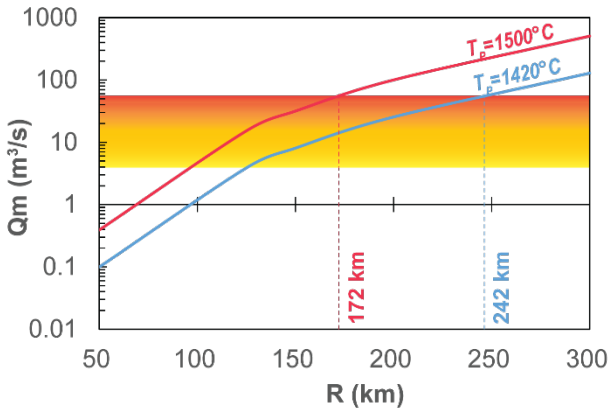

Figure S16. Magma flux as a function of plume radius. Magma flux (Q_m, in m^3/s) as a function the radius of the plume (R) for T_P = 1500 °C (the maximal estimated value in this study) and T_P = 1420°C (Borchardt & Lee, 2022). The colored box shows the range of estimated magmatic flux for the Icelandic plume between 54 and 40 My (Mjelde & Faleide, 2009). The dashed lines show the plume radius required to produce Qm = 55 m^3/s.